White Matter Models of *In Vivo* Diffusion MRI Human Brain Data: A Statistical Ranking

Uran Ferizi[12]
u.ferizi@cs.ucl.ac.uk
Eleftheria Panagiotaki[1]
e.panagiotaki@cs.ucl.ac.uk
Torben Schneider[2]
t.schneider@ucl.ac.uk
Claudia Wheeler-Kingshott[2]
c.wheeler-kingshott@ucl.ac.uk
Daniel Alexander[1]
d.alexander@ucl.ac.uk

[1] Centre for Medical Image Computing
Department of Computer Science
University College London
London, UK

[2] NMR Research Unit
Department of Neuroinflammation
Institute of Neurology
University College London
London, UK

Abstract

Diffusion MRI (Magnetic Resonance Imaging) Microstructure Imaging provides a unique non-invasive probe into the microstructure of biological tissue. However, it relies on a mathematical model relating microscopic tissue features to the MR signal. This work aims to determine which models of diffusion MRI are best at describing the signal from *in vivo* brain white matter. The assumption of Gaussian diffusion in the most commonly used model, the Diffusion Tensor, oversimplifies the diffusive behaviour of water in complex media and is known to break down for relatively large diffusion weights (b-values). Recent work shows that three-compartment models, incorporating restricted intra-axonal compartments, glial compartments and hindered extra-cellular diffusion, are best at explaining multi b-value data sets from fixed brain tissue. Here we perform a similar experiment using *in vivo* human data to avoid, and evaluate, the effects of the fixation process. We compare one-, two- and three-compartment models, and rank them using two standard model selection criteria. Results show that, as with fixed tissue, three-compartment models explain the data best, although simpler models emerge from the *in vivo* data. Both changes in diffusion behaviour from fixation and the lower gradient strengths available *in vivo* are likely to contribute to the difference. The full ranking assists the choice of model and imaging protocol for future brain microstructure imaging.

1 Introduction

Diffusion MRI measures the water dispersion in biological tissue and can therefore be used to probe the microstructure. Though useful in other tissue types, this technique is most often applied in the brain, especially where parallel fibres restrict water mobility anisotropically, thus providing putative measures of white matter integrity and connectivity.

Currently, the standard model for imaging diffusion in tissue is the Diffusion Tensor (DT) [7], which assumes a trivariate Gaussian dispersion pattern. Derived indices, such as Mean

Diffusivity (MD) and Fractional Anisotropy (FA), can correlate with major tissue damage, but lack the sensitivity and specificity to provide indices such as axon radius, density, orientation, dispersion and permeability, which potentially give much greater insight into tissue architecture and pathology. These can be estimated by applying more complex models to richer data sets [2, 3, 4, 5, 6, 12, 14, 15].

Stanisz et al. [14] pioneered a multi-compartment representation of the separate diffusive processes in nerve tissue. The Ball-Stick model [8] is the simplest possible two-compartment model with restricted axonal diffusion and isotropic extra-axonal diffusion. The CHARMED model (Composite Hindered and Restricted Model of Diffusion) [4] is a similar two-compartment model that allows anisotropic Gaussian Diffusion in the 'hindered' extra-cellular space and non-zero-radius cylindrical intra-cellular diffusion. The AxCaliber technique [5] extended the CHARMED model to estimate the distribution of axon diameters. Barazany et al. [6] demonstrated the approach *in vivo* on a rat's Corpus Callosum (CC), adding a third free-diffusion compartment to account for Cerebrospinal Fluid (CSF) contamination. Alexander et al. [2] used a similar model to derive orientationally invariant indices of axon diameter and density.

Increasing model complexity can potentially lead to overfitting and false parameter estimation. Recently, Panagiotaki et al. [12] compared 47 diffusion MRI models using data from fixed White Matter (WM) of rats, using the Bayesian Information Criterion (*BIC*). They proposed a taxonomy of one-, two- and three- compartment models as a combination of: i) a hindered/extra-cellular diffusion via a Tensor (an ellipsoid), a Zeppelin (a cylindrically symmetric ellipsoid) or a Ball (an isotropic sphere); ii) a restricted/intra-cellular diffusion via a Stick (an oriented line with zero radius), a Cylinder (a Stick with non-zero constant radius) or Gamma Distributed Cylinders (not included in this work); iii) an isotropically restricted component, representing glial cells or isotropically oriented axons, modelled by a Dot ("stationary" water), a Sphere (spherically restricted), Astrosticks (zero radius lines isotropically spread in space) or Astrocylinders (similarly to the Astrosticks, but with non-zero radii). They concluded that the three-compartment models perform best and DT worst.

Here we repeat the experiment in [12] using *in vivo* data from the human brain's CC and the software used in [12] as part of the Camino toolkit [10]. We acquire a rich data set with many combinations of diffusion and gradient times and gradient magnitudes to fit the models to as wide a fraction of the measurement space as possible. We test the quality-of-fit of models to the data using *BIC*, and confirm with the Akaike Information Criterion (*AIC*).

2 Methods

This section describes the acquisition protocol for our rich data set and outlines the preprocessing we perform to obtain a set of measurements for model fitting. It then details the fitting procedure and the techniques we use for model selection and ranking.

2.1 DW/DT Acquisition

Using a 3T Phillips scanner, we scan a 30-year old healthy man, using three gradient-encoding directions: one approximately along CC main fiber direction and two in its perpendicular plane. The images consist of 8x4mm sagittal slices, an image size of 64x64 and in-plane resolution of 2mm x 2mm.

Using a Pulsed-Gradient-Spin-Echo sequence, we probe gradient strengths |G| = 30, 40, 50, 60 mT/m, gradient times δ = 5, 15, 25ms, and diffusion times Δ ranging in steps of 10ms, from 20 to 100ms. This produces a total of 63 diffusion weightings, excluding any combinations where δ>Δ, with maximum weight b=8,300s/mm^2. As the echo times vary across different acquisition parameters, in addition to every diffusion-weighted acquisition we obtain a corresponding non-diffusion-weighted (b=0) one. We also perform a separate HARDI (High Angular Resolution Diffusion Imaging) acquisition with the same image resolution, 32-gradient encoding directions and b=711s/mm^2. The total acquisition time is 2.5hrs.

2.2 Data Preprocessing

As in [12], we first fit the DT model to the HARDI data and find the principal direction to identify voxels containing fibres well aligned with the assumed fibre direction. We take all voxels with FA above a threshold and principal eigenvector within a small angle of tolerance of the assumed fiber direction and average them to give a single data set to which the model can be fitted. Here, we set the FA threshold at 0.5 and repeat the experiment with three different angular thresholds, 2°, 5° and 10°, to establish the effect of orientation dispersion. For b>3,500s/mm^2, the parallel direction signal reaches the noise floor, so we exclude these data, thus leaving us with 171 DW (and 63 unweighted) images. The SNR is about 20. The signal at each DW is normalised by the corresponding diffusion-unweighted measurement with the same echo time, to remove T2 effects, before the fitting.

2.3 Model Fitting

We fit 32 models of diffusion to the signal, using the open software tool Camino [10]. We fit in two stages: after an initial run of 1,000 random starting points, we extract the parameters that produce the minimum objective function. We then execute another 1,000 runs from starting points at small random perturbations from the first minimum. This ensures that we avoid local minima and obtain the best fit parameters. The offset-Gaussian noise model is used, as in [12], to construct the objective function to minimize (*RES*). This objective function accounts for bias introduced by the Rician noise inherent in the data in a simplistic way [11] that is more numerically stable than a full Rician log-likelihood objective function.

2.4 Model Selection

Model selection criteria, as introduced in [13]

$$BIC = -2\log(L) + K\log(N) \tag{1}$$

where L is the likelihood of obtaining the present data given the model, K is the number of free parameters and N is the number of measurements, or in [1]

$$AIC = -2\log(L) + 2K + \frac{2K(K+1)}{(N-K-1)} \tag{2}$$

quantify the trade-off between complexity and goodness-of-fit to identify the simplest model that explains some data. The lower the scores, the more predictive the model is. The last term in the *AIC* is the adaptation suggested in [9] of the original *AIC* for cases where the number of measurements is not large (deemed to be smaller than about 40 times the number of free parameters). In general, the *AIC* is less conservative in penalising complexity.

Parameters	Model	2° deviation BIC order	2° deviation AIC order	2° deviation RES	5° deviation BIC order	5° deviation AIC order	5° deviation RES	10° deviation BIC order	10° deviation AIC order	10° deviation RES
6	Ball.Stick.Ast	**1**	1	149.05	**1**	1	94.54	**1**	1	74.41
6	Ball.Stick.Dot	**2**	6	151.64	**2**	6	96.44	**2**	6	76.61
7	Ball.Stick.Acl	**3**	2	149.05	**5**	2	94.29	**6**	2	73.73
7	Ball.Cylin.Acl	**4**	3	149.06	**3**	3	94.23	**4**	3	73.52
7	Ball.Cylin.Ast	**5**	4	149.06	**4**	4	94.28	**5**	4	73.61
7	Zepp.Stick.Ast	**6**	5	149.07	**6**	5	94.48	**3**	5	73.48
5	Ball.Stick	**7**	21	162.38	**7**	21	106.82	**9**	21	87.00
7	Zepp.Stick.Dot	**8**	10	151.64	**8**	10	95.97	**7**	10	74.83
7	Ball.Cylin.Dot	**9**	11	151.65	**9**	11	96.16	**8**	11	75.79
7	Ball.Stick.Sph	**10**	12	151.86	**10**	12	96.41	**10**	12	76.51
8	Zepp.Stick.Acl	**11**	7	149.08	**13**	7	94.24	**13**	7	72.99
8	Zepp.Cylin.Acl	**12**	8	149.09	**11**	8	94.19	**12**	8	72.89
8	Zepp.Cylin.Ast	**13**	9	149.14	**12**	9	94.23	**11**	9	72.89
6	Ball.Cylin	**14**	24	162.38	**15**	24	106.60	**17**	24	86.33
6	Zepp.Stick	**15**	25	162.39	**14**	25	105.80	**15**	25	85.44
8	Zepp.Cylin.Dot	**16**	14	151.64	**16**	14	95.72	**14**	14	74.21
8	Ball.Cylin.Sph	**17**	15	151.76	**18**	15	96.16	**18**	15	75.79
8	Zepp.Stick.Sph	**18**	16	151.77	**17**	16	95.92	**16**	16	74.62
9	Tens.Stick.Ast	**19**	13	149.09	**19**	13	94.46	**19**	13	73.43
9	Tens.Stick.Dot	**20**	17	150.96	**23**	17	96.27	**23**	17	76.30
7	Zepp.Cylin	**21**	27	162.39	**20**	27	105.57	**20**	27	84.85
7	Bizepp.	**22**	28	162.39	**21**	28	105.80	**22**	28	85.44
9	Zepp.Cylin.Sph	**23**	20	153.48	**22**	20	95.72	**21**	20	74.20
10	Tens.Cylin.Acl	**24**	18	149.09	**26**	18	94.21	**25**	18	72.97
10	Tens.Stick.Acl	**25**	19	149.14	**25**	19	94.16	**24**	19	72.79
8	Tens.Stick	**26**	30	162.41	**24**	30	105.21	**27**	30	84.68
10	Tens.Cylin.Dot	**27**	22	151.72	**28**	22	95.65	**28**	22	74.17
10	Tens.Stick.Sph	**28**	23	152.30	**29**	23	95.86	**29**	23	74.58
9	Tens.Cylin	**29**	31	162.56	**30**	31	105.09	**30**	31	84.48
10	Tens.Cylin.Ast	**30**	29	157.64	**27**	29	95.40	**26**	29	73.18
11	Tens.Cylin.Sph	**31**	26	152.29	**31**	26	95.69	**31**	26	74.17
7	Tensor	**32**	32	616.71	**32**	32	477.12	**32**	32	449.85

(a)

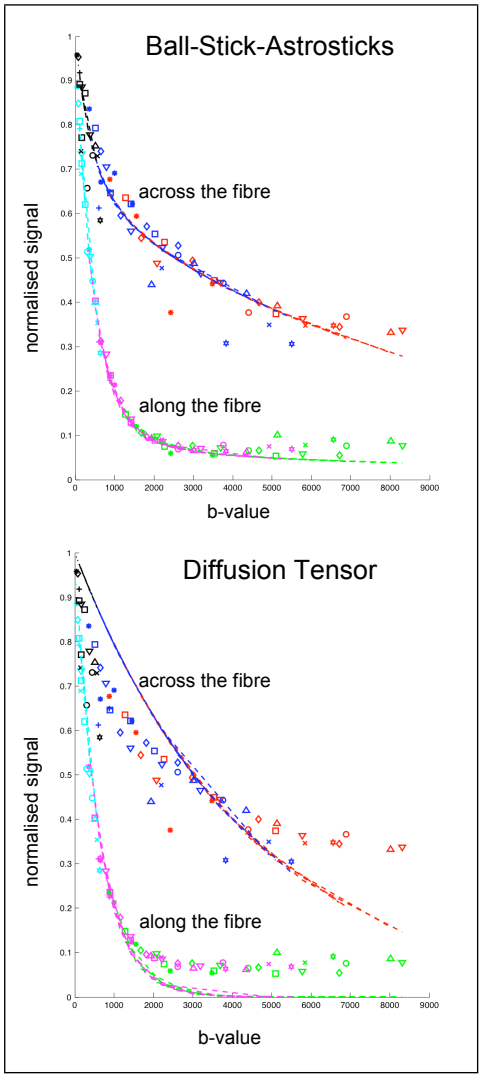

(b)

Figure 1: a) Models ranked for the 2°/5°/10° fibre deviation allowances. Adjacent are the raw scores for their respective Objective Function Residue (*RES*). The Ball-Stick-Astrosticks does best across both *BIC* and *AIC*, the DT worst. (Abbrev.: Tens.=Tensor; Zepp.=Zeppelin; Cylin.=Cylinder; Ast.=Astrosticks; Acl.=Astrocylinders; Sph.=Sphere). b) Matching the raw signal and the signal synthesized from the model parameters for the 2° threshold data set. The Ball-Stick-Astrosticks model fits the data well; the Tensor (DT) fits poorly.

3 Results

The ranking of the models is provided in the table of Fig.1, separately for 2°, 5° and 10° angular threshold data sets, for both *BIC* and *AIC* . The models are listed according to the *BIC* performance in the 2° data set. We also give the raw scores for the *BIC*, *AIC* and *RES*.

The three compartment models describe the data best. The single compartment model, the DT, performs worst across all criteria. The most complex model, the Tensor-Cylinder-Astrocylinders, gives small *RES*, but its complexity is penalised under *AIC*, more under *BIC*.

In the extra-cellular space, the Ball, the Zeppelin and the Tensor perform equally well, judged on their *RES* score, but the simpler Ball scores better on *BIC*. The intracellular Stick does best with *BIC*, but Cylinders perform well too, especially across all 3 scores (e.g. Ball-Cylinder-Astrocylinders). Across the third compartments, the Sphere performs worst, partly because of its model complexity.

The *RES* scores decrease markedly as the orientation threshold increases from 2° to 5°, but at a smaller rate from 5° to 10°. This suggests that the models fit increasingly better as the number of voxels averaged increases.

The plots of Fig.1 show the fit of two models, the best and the worst from the ranking, to the data, revealing the limitations of the overly simple single-compartment DT model. The DT model cannot capture the shape of the perpendicular signal decay because it does not model restriction. The three-compartment model, Ball-Stick-Astrosticks, fits both the parallel and perpendicular direction signal decay closely.

4 Discussion

By using a wide range of diffusion weights and times, we showed that standard models from the literature, such as the DT and Ball-Stick, are too simple to describe diffusion in the brain. Three compartments are required to explain the diffusion in white matter *in vivo*. These models fit the data best, with very similar precision, and the simpler members of this class are favoured under the BIC ranking. Further work with high angular resolution data sets will shed more light on this.

The *BIC* for the Cylinder models are only marginally lower than those of Stick, supporting a future use of cylinder models for estimating axon diameter *in vivo*, as in [3, 6, 15].

For the third compartment, the Astrosticks or Astrocylinders show an advantage over the Sphere and Dot, which were favoured for fixed tissue in [12]. This could be because of intrinsic differences between live and fixed tissue, or differences in the imaging protocol, since we use much lower gradient strength. Intrinsic tissue differences are a likely cause; Alexander in [3] suggests fixation may make membranes 'stickier', giving rise to slow moving water well captured by the Dot model.

Minor variations in the dispersion of fibre direction in the data set affect fitting quality, since the models we test here capture either no dispersion or a fully uniform one. We intend to consider localised dispersion in future work using, for example, the models in [15]. The Astrosticks and Astrocylinders models may improve the fit simply by accommodating small amounts of fibre orientation dispersion even at the 2° threshold, or may genuinely capture a small population of fibres with uniformly distributed orientation.

We also emphasize that the choice of models our analysis suggests is not appropriate for existing sparse data sets such as off-the-shelf single shell HARDI data which only support simple models. Rather, these results inform the choices for future *in vivo* microstructure imaging once we identify the right model. Experiment design techniques such as [2] can determine economical protocols. We emphasize that the protocol we use here is designed specifically for model selection rather than large scale application.

As, intentionally, we conservatively selected the part of the CC that is mostly homogeneous, with little fibre crossing or CSF contamination, other models may perform better across or away from the CC (e.g. a CSF pool as in [6]). Future work will include other models such as a distribution of pore sizes [5, 12] and orientation [15].

5 Acknowledgements

EPSRC kindly funds the Research Studentship of U.Ferizi. We are grateful to the Multiple Sclerosis Society of Great Britain and Northern Ireland for supporting the NMR unit.

This work was undertaken at UCLH/UCL who received a proportion of funding from the Department of Health NIHR Biomedical Research Centres funding scheme.

References

[1] H. Akaike. A new look at the statistical model identification. *Automatic Control, IEEE Transactions on*, 19(6):716–723, 1974.

[2] D.C. Alexander. A general framework for experiment design in diff. MRI and its application in measuring direct tissue-microstructure features. *MRM*, 60(2):439–448, 2008.

[3] D.C. Alexander, P.L. Hubbard, M.G. Hall, E.A. Moore, M. Ptito, G.J.M. Parker, and T.B. Dyrby. Orientationally invariant indices of axon diameter and density from diffusion MRI. *NeuroImage*, 52(4):1374–1389, 2010.

[4] Y. Assaf, R.Z. Freidlin, G.K. Rohde, and P.J. Basser. New modeling and experimental framework to characterize hindered and restricted water diffusion in brain white matter. *Magnetic Resonance in Medicine*, 52(5):965–978, 2004.

[5] Y. Assaf, T. Blumenfeld-Katzir, Y. Yovel, and P.J. Basser. Axcaliber: a method for measuring axon diameter distribution from diff. MRI. *MRM*, 59(6):1347–1354, 2008.

[6] D. Barazany, P.J. Basser, and Y. Assaf. In vivo measurement of axon diameter distribution in the corpus callosum of rat brain. *Brain*, 132(5):1210, 2009.

[7] P.J. Basser, J. Mattiello, and D. LeBihan. MR diffusion tensor spectroscopy and imaging. *Biophysical journal*, 66(1):259–267, 1994.

[8] TEJ Behrens, MW Woolrich, M. Jenkinson, H. Johansen-Berg, RG Nunes, S. Clare, PM Matthews, JM Brady, and SM Smith. Characterization and propagation of uncertainty in diffusion-weighted MR imaging. *MRM*, 50(5):1077–1088, 2003.

[9] K.P. Burnham and D.R. Anderson. Kullback-Leibler information as a basis for strong inference in ecological studies. *Wildlife Research*, 28(2):111–119, 2001.

[10] PA Cook, Y. Bai, S. Nedjati-Gilani, KK Seunarine, MG Hall, GJ Parker, and D.C. Alexander. Camino: Open-source diffusion-MRI reconstruction and processing. In *14th scientific meeting of the ISMRM*, volume 2759, 2006.

[11] D.K. Jones and P.J. Basser. "Squashing peanuts and smashing pumpkins": How noise distorts DW-MR data. *MRM*, 52(5):979–993, 2004.

[12] E. Panagiotaki, T. Schneider, B. Siow, M.G. Hall, M.F. Lythgoe, and D.C. Alexander. Compartment models of the diffusion MR signal in brain white matter: A taxonomy and comparison. *NeuroImage*, 2011.

[13] G. Schwarz. Estimating the dimension of a model. *The A. of Stat.*, 6(2):461–464, 1978.

[14] G.J. Stanisz, G.A. Wright, R.M. Henkelman, and A. Szafer. An analytical model of restricted diffusion in bovine optic nerve. *MRM*, 37(1):103–111, 1997.

[15] H. Zhang, P.L. Hubbard, G.J.M. Parker, and D.C. Alexander. Axon diameter mapping in the presence of orientation dispersion with diffusion MRI. *NeuroImage*, 2011.